Available online at website: https://journal.bcrec.id/index.php/bcrec

Bulletin of Chemical Reaction Engineering & Catalysis, 21 (4) 2026, 781-797

Original Research Article

Effect of SiO_2, ZrO_2, and SiO_2-ZrO_2 Supports on Product Distribution in Glucose Hydrogenolysis over Cu-Ni-WO_x Catalysts

Ahmad Sholeh Romdlon[1], Yuniar Ponco Prananto[1], Siti Mariyah Ulfa[1,2] *

[1]*Department of Chemistry, Faculty of Mathematics and Natural Sciences, Brawijaya University, Jl. Veteran, Malang, East Java, Indonesia.*
[2]*Synthesis and Catalysis of Natural Product Research Group, Faculty of Mathematics and Natural Sciences, Brawijaya University, Jl. Veteran, Malang, East Java, Indonesia.*

Received: 2nd May 2026; Revised: 16th July 2026; Accepted: 17th July 2026
Available online: 22th July 2026; Published regularly: December 2026

Abstract

Biomass-derived glucose is an important platform molecule to produce value-added oxygenated chemicals through catalytic conversion. In this study, Cu-Ni-WO_x catalysts supported on SiO_2, ZrO_2, and SiO_2-ZrO_2 were prepared by wet impregnation and evaluated for the hydrogenolysis of glucose in water. The catalysts were characterized by X-ray diffraction, SEM-EDX, and pyridine-adsorption FTIR to examine the relationship between catalyst structure, acidity, and catalytic behavior. Catalytic tests were carried out in a batch reactor at 300 °C under 2 MPa H_2 for 2 h. All catalysts showed comparable glucose conversion in the range of 92.2-93.1%, whereas the support strongly influenced the distribution of liquid products. The SiO_2-supported catalyst favored glycol/glycol-like compounds and cyclic ether/THF products, indicating a stronger tendency toward oxygen-retaining pathways. In contrast, the SiO_2-ZrO_2-supported catalyst showed higher distribution toward cyclic ketones and aliphatic alcohols, while the ZrO_2-supported catalyst exhibited an intermediate pattern. These findings suggest that support-dependent acidity plays an important role in directing hydrogenolysis pathways and controlling the relative formation of oxygen-retaining and rearranged products. This work highlights the importance of support composition in tuning the product distribution of Cu-Ni-WO_x catalysts for glucose valorization into value-added oxygenates.

Keywords: Cu-Ni-WOx catalyst; metal oxide support; glucose hydrogenolysis; aliphatic alcohol; cyclic ether; glycol-like compounds

How to Cite: Romdlon, A. S., Prananto, Y. P., Ulfa, S. M. (2026). Effect of SiO_2, ZrO_2, and SiO_2-ZrO_2 Supports on Product Distribution in Glucose Hydrogenolysis over Cu-Ni-WOx Catalysts. *Bulletin of Chemical Reaction Engineering & Catalysis*, 21 (4), 781-797. (DOI: 10.9767/bcrec.20724)

Permalink/DOI: https://doi.org/10.9767/bcrec.20724

Supporting Information: https://journal.bcrec.id/index.php/bcrec/article/downloadSuppFile/20724/6547

1. Introduction

Biomass is one of the most abundant renewable carbon resources and has attracted considerable attention as a feedstock for the sustainable production of fuels and value-added chemicals. Among biomass-derived intermediates, glucose is a particularly important platform molecule because it can be obtained from the hydrolysis of cellulose and subsequently converted into a wide range of oxygenated products through catalytic processes [1,2]. Depending on the catalyst properties and reaction conditions, glucose hydrogenolysis may proceed through hydrogenation, hydrogenolysis, dehydration, rearrangement, and retro-aldol pathways, producing compounds such as glycols, cyclic ketones, cyclic ethers, and aliphatic alcohols. Recent studies have shown that product selectivity in glucose hydrogenolysis can vary significantly, with glycol yields typically reported in the range of 40-70%, cyclic ketones around 20-40%, and aliphatic alcohols approximately 15-35%, depending on catalyst composition and acidity [3].

A clear understanding of catalyst structure and reaction pathways is essential for the rational

* Corresponding Authors.
Email: ulfa.ms@ub.ac.id (S. M. Ulfa)

design of efficient catalytic systems for biomass valorization. In heterogeneous catalysis, catalytic performance is strongly influenced by the nature of the active metal species, the promoter, and the support. Transition metals such as Ni and Cu are widely used in biomass conversion because they provide complementary catalytic functions, that is enhance reaction efficiency and selectivity [4,5]. Nickel is effective for H_2 activation and hydrogenolysis-related reactions, whereas Cu is often associated with hydrogenation and selective transformation of oxygenated intermediates. The active interface between metal species and oxide supports is particularly important because it provides adsorption sites and low-energy reaction pathways for C–H bond activation and C–C bond cleavage [6].

In addition to the active metals, support composition plays a decisive role in controlling metal dispersion, acidity, and metal-support interaction. SiO_2 is generally characterized by high surface area and good thermal stability, while ZrO_2 provides Lewis and Brønsted acidic properties that are beneficial for biomass conversion reactions involving dehydration, rearrangement, and C-O bond activation [7-10]. Mixed SiO_2-ZrO_2 supports are especially attractive because they may combine the structural advantages of silica with the acid-base functionality of zirconia, thereby offering a tunable environment for selective glucose conversion.

The catalytic behavior of Cu- and Ni-based systems in biomass transformation has been reported extensively. Ni-based catalysts have shown high activity in the conversion of oxygenated biomass-derived into HMF reaching 88.5% yield. The performance enhanced by modification into NiZn and produce DMF up to 93.6% [11,12]. Cu-based catalysts have also been reported to be highly effective in hydrogenolysis and hydrogenation reactions, particularly when strong interactions between Cu species and oxide supports are established, e.g., the Cu–O–Si system can achieve DMF selectivity of up to 93.4% [13]. The development of CuNi bimetallic catalysts is therefore attractive because Cu may facilitate activation of C=O containing intermediates, while Ni contributes to H_2 activation, producing a synergistic catalytic system with modified electronic properties and improved performance [14-16].

The incorporation of tungsten oxide species has also been reported to influence catalytic performance in biomass-related transformations. Tungsten-based catalysts may facilitate C-C bond cleavage and promote the formation of smaller oxygenated intermediates, while WO_x may also modify the oxidation state and electronic environment of Cu-containing catalysts [17,18]. Despite the relevance of Cu-, Ni-, and W-based catalysts for biomass conversion, the support-dependent behavior of Cu-Ni-WO_x catalysts in glucose hydrogenolysis remains insufficiently understood, particularly with respect to how SiO_2, ZrO_2, and SiO_2-ZrO_2 supports influence catalyst acidity and product distribution.

In this study, Cu-Ni-WO_x catalysts supported on SiO_2, ZrO_2, and SiO_2-ZrO_2 were prepared by wet impregnation and evaluated in the hydrogenolysis of glucose in water. The objective of this work was to clarify how support composition influences catalyst structure, acidity, glucose conversion, and liquid product selectivity. We hypothesized that differences in support composition would modify the Lewis-Brønsted acidity balance and metal-support interaction, thereby redirecting the reaction pathways of glucose hydrogenolysis and altering the relative formation of cyclic ketones, glycol/glycol-like compounds, aliphatic alcohols, and cyclic ether products.

2. Materials and Methods

2.1. Materials

Analytical-grade D-(+)-glucose (Merck KGaA) was used as the primary starting material. The $Cu(NO_3)_2.3H_2O$, $Ni(NO_3)_2.6H_2O$, $ZrOCl_2.8H_2O$, SiO_2 (Merck KGaA), and $Na_2WO_4.2H_2O$ (SMART-LAB) were employed as precursors for the synthesis of Cu-Ni-WO_x catalyst and SiO_2-ZrO_2-based support. Ammonium hydroxide solution (NH_4OH), silver nitrate solution ($AgNO_3$), and nitric acid (HNO_3), all obtained from Merck were used during the catalyst preparation. Nitrogen and hydrogen gases were purchased from PT. Tira Austenite Tbk. Deionized water Hydrobath from local distributors were used as the solvent in the catalyst preparation and catalytic test for glucose hydrogenolysis.

2.2. Catalyst Preparation

Three catalysts were prepared in this study, namely MSZ (Cu-Ni-WO_x/SiO_2-ZrO_2), MS (Cu-Ni-WO_x/SiO_2), and MZ (Cu-Ni-WO_x/ZrO_2), using a wet impregnation method with several modifications based on previous studies [19-22]. For the preparation of the SiO_2-ZrO_2 support, $ZrOCl_2 \cdot 8H_2O$ was precipitated with NH_4OH to pH of 8, producing a white solid. The precipitate was washed, dried, and subsequently combined with SiO_2, followed by stirring at 75 °C for 24 h. The material was evaporated, dried, and calcined at 500 °C under N_2. Tungsten precursor was then introduced by impregnation using $Na_2WO_4.2H_2O$ under acidic conditions by adjusting the pH to 1 with HNO_3. Afterward, Cu and Ni precursors were added under basic conditions at pH of 11. The resulting material was stirred for 24 h,

evaporated, dried, calcined, and reduced at 500 °C under H_2 to obtain the MSZ catalyst. The MS catalyst was prepared using commercial SiO_2 as the support. The synthesis followed a similar procedure, including tungsten impregnation under acidic conditions, addition of Cu and Ni precursors under basic conditions, evaporation, drying, calcination at 500 °C in N_2, and reduction at 500 °C with H_2. For the MZ catalyst, ZrO_2 was first prepared by precipitation using NH_4OH to pH of 8, followed by drying and calcination at 500 °C. The resulting ZrO_2 was then impregnated with Cu, Ni, and W precursors under basic conditions, followed by stirring, evaporation, drying, calcination, and hydrogen reduction to obtain the final catalyst.

2.3. Catalyst Characterizations

The crystalline structure of the catalysts was analyzed by X-ray diffraction (XRD) using a PANalytical X'Pert3 Powder diffractometer operated at 40 kV and 35 mA with Cu-Kα radiation (λ = 1.54060 Å). Diffraction patterns were recorded over a 2θ range of 10° to 90°. The obtained XRD patterns were subsequently analyzed by Rietveld refinement using Profex software (version 5.7.1) with the BGMN refinement engine to identify the crystalline phases and determine their quantitative phase composition. Surface morphology and elemental distribution were examined by SEM-EDX using an FEI Quanta FEG 650 FE-SEM equipped with an Oxford Instruments X-act detector and AZtecOne software. Catalyst acidity was evaluated by pyridine-adsorption FTIR [23-25]. Pyridine was used as a probe molecule to distinguish Lewis and Brønsted acid sites. Absorption bands near 1446 cm^{-1} were assigned to pyridine coordinated to Lewis acid sites, while bands near 1544 cm^{-1} were attributed to pyridinium species associated with Brønsted acid sites. The band around 1484 cm^{-1} was associated with pyridine interacting with both Lewis and Brønsted acid sites.

2.4. Catalytic Hydrogenolysis of Glucose

Catalytic hydrogenolysis of glucose was performed in a 100 mL stirred batch autoclave reactor, as illustrated in Figure 1. First, 0.6 g of catalyst was activated in situ at 300 °C for 1 h under an H_2 atmosphere. After cooling, 1 g of glucose and 25 mL of deionized water were introduced into the reactor. The reactor was sealed and purged three times with N_2, then pressurized with H_2 to 2 MPa. The reaction was carried out at 300 °C for 2 h at a stirring speed of 400 rpm. After the reaction, the reactor was cooled to room temperature, and the gaseous phase was released. The liquid products were collected from the condensate chamber and further distilled at 79-89 °C to separate the target fraction from water before analysis.

2.5. Product Analysis

The liquid products were analyzed by GC-MS using a Shimadzu QP2020NX equipped with an SH-PolarWax polyethylene glycol column. The oven temperature was initially set at 80 °C and increased to 250 °C. Samples were injected in splitless mode using helium as the carrier gas. For analysis, 0.5 mL of liquid product was diluted with 0.5 mL of GC-grade *n*-BuOH as an internal standard. Compounds were identified using the NIST mass spectral library, and the relative chromatographic area fractions used to evaluate trens of each product distribution among the prepared catalysts.

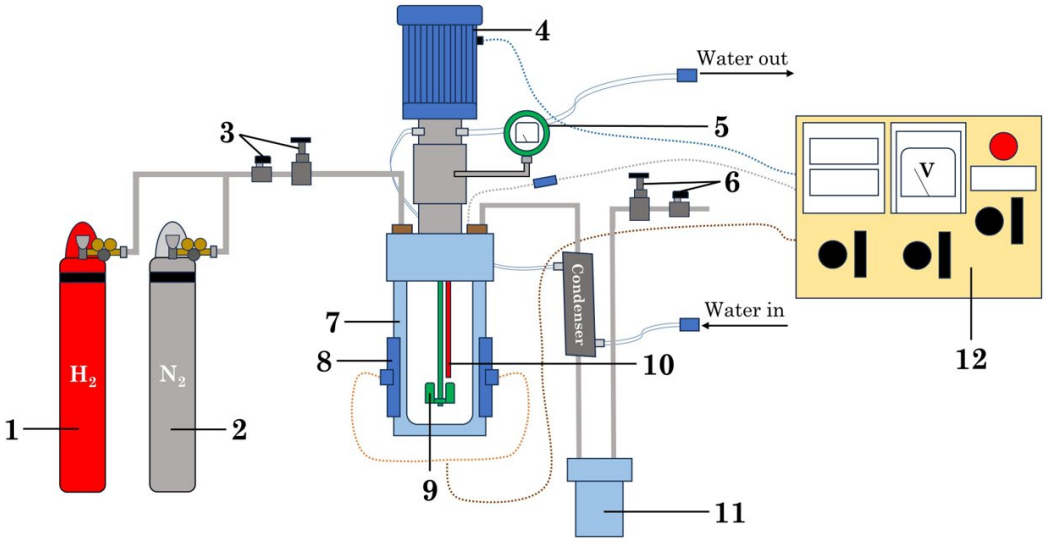

Figure 1. Schematic diagram of batch-autoclave reactor: (1) hydrogen cylinder; (2) nitrogen cylinder; (3) gas inlet valves; (4) impeller motor; (5) pressure gauge; (6) gas outlet valves; (7) autoclave reactor; (8) heater; (9) impeller; (10) thermocouple; (11) condensate collector; and (12) reactor controller.

Glucose conversion was determined from the reducing sugar content using the DNS method [26]. The sample was reacted with DNS reagent, heated at 95 °C for 5 min, and the absorbance was measured at 540 nm using a UV-Vis spectrophotometer. A D-glucose calibration curve was used for quantification. Glucose conversion, relative products distribution, and carbon balance were calculated as follows:

$$\text{Conversion (\%)} = \frac{\text{n}_0 \text{ of glucose} - \text{n}_\text{f} \text{ of glucose}}{\text{n}_0 \text{ of glucose}} \times 100\% \quad (1)$$

where n_0 is the initial number of glucose and n_f is the amount of glucose remaining after the reaction:

$$\text{Relative products distribution (\%)} = \frac{\text{Area of desired product}}{\text{Area of total product}} \times 100\% \quad (2)$$

$$\text{Carbon balance (\%)} = \frac{(\text{C}_\text{unreact} \text{ of glucose} + \text{C}_\text{isolated} \text{ of liquids})}{\text{C}_0 \text{ of glucose}} \times 100\% \quad (3)$$

where C_0 is the carbon of initial glucose; $C_{unreact}$ is the carbon of unreacted glucose; $C_{isolated}$ is the sum of carbon from isolated liquids products. The relative products distribution and carbon balance is calculated based on GC-MS analysis.

3. Results and Discussion

3.1. Catalyst Characterizations

Overall, the results of XRD analysis and phase quantification indicate that the type of support has a significant influence on the composition and crystal structure of the catalyst, as shown in Figure 2. The SiO_2 support maintains amorphous character and promotes the formation of Ni_2SiO_4, while the ZrO_2 support produces high crystallinity and facilitates the formation of Cu-Ni alloys. In the SiO_2-ZrO_2 composite catalyst, the presence of *t*-ZrO_2 and amorphous SiO_2 coexist with the formation of Ni_2SiO_4, indicating strong interactions between the support and active metals. The coexistence of crystalline and amorphous phases is expected to modify the textural properties and metal-support interactions. Previous studies have shown that amorphous SiO_2-ZrO_2 supports possess both Lewis and Brønsted acid sites, with their distribution strongly influenced by the merging of SiO_2-ZrO_2. In addition, higher surface area and smaller Ni° particle size on silica-zirconia supports have been associated with improved metal dispersion. Therefore, the observed phase composition is expected to contribute to enhanced surface acidity, active metal dispersion, and catalytic activity during glucose hydrogenolysis [27,28].

The diffraction pattern of MSZ (Cu-Ni-WO_x/SiO_2-ZrO_2) catalyst shows dominant peaks corresponding to the tetragonal ZrO_2 phase at approximately 2θ = 30°, 35°, 50°, and 60°, accompanied by a broad SiO_2 band at approximately 22° indicating the amorphous character of the SiO_2-ZrO_2 composite support. In addition to the support phase, the presence of Ni_2SiO_4 and reduced tungsten species $WO_{2.72}$ were also identified, while the WO_2 phase was not detected. The Rietveld quantification results showed the active phase composition of 12.85 wt.% Ni_2SiO_4, 3.85 wt.% $WO_{2.72}$, and 0.92 wt.% Cu°. The presence of $WO_{2.72}$ indicates that tungsten is in a lower oxidation state. However, the formation of Na_2SiO_4, as well as the absence of Cu-Ni alloy phase, is due to the high dispersion of the metal and the small size of the crystallites formed on the support surface [29].

In the MS (Cu-Ni-WO_x/SiO_2) catalyst, the diffraction pattern is dominated by a broad band typical of amorphous SiO_2 around 2θ = 22°, indicating a low degree of crystallinity of the silica support. This peak broadening indicates a lack of crystal regularity and possibly very small crystallite sizes or high dispersion of active species on the SiO_2 surface. Several weak peaks associated with WO_2 and Ni_2SiO_4 are still observed, while the Cu-Ni alloy phase is not detected because of the high metal dispersion on the low crystallite support. Quantification results showed that SiO_2 was the dominant phase (81.17

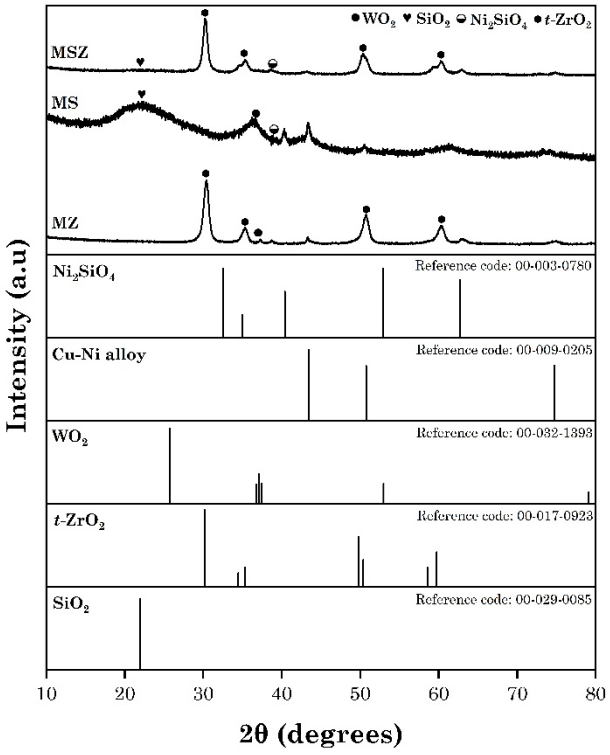

Figure 2. X-ray diffraction of the catalysts, illustrating the effect of different support compositions on the crystalline structure and phase distribution.

wt.%), followed by Ni_2SiO_4 (11.66 wt.%), WO_2 (2.93 wt.%), $WO_{2.72}$ (2.91 wt.%), and Cu° (1.33 wt.%), as shown in Table 1. The high dispersion of Cu and WO_x species on the amorphous support potentially increases the number of exposed active sites, while the formation of Ni_2SiO_4 indicates that some Ni interacts strongly with SiO_2, thereby having profound implications for the catalytic properties of the material, particularly regarding the reducibility of nickel species [30].

In contrast, the MZ (Cu-Ni-WO_x/ZrO_2) catalyst exhibited sharp diffraction peaks dominated by *t*-ZrO_2, indicating higher crystallinity compared to MSZ and MS. Furthermore, the presence of WO_2, $WO_{2.72}$, Cu, and a Cu-Ni alloy was identified. Quantitative analysis shows that *t*-ZrO_2 dominates the phase composition (93.48 wt.%), followed by Cu (2.73 wt.%), Cu-Ni alloy (1.96 wt.%), $WO_{2.72}$ (1.28 wt.%), and WO_2 (0.55 wt.%) (Table 1). The formation of Cu-Ni alloy indicates a good interaction between the two metals during reduction, thus potentially providing more active hydrogenation sites. Nevertheless, the presence of WO_x species is thought to contribute as an oxyphilic site that supports the activation of C–O bonds in the hydrogenolysis reaction [31]. This contrasts with silica-supported catalysts where the formation of Ni_2SiO_4 can limit the availability of metallic nickel sites, thereby reducing hydrogenation capacity. In the MZ catalyst, the absence of such strong, inhibiting support interactions allows for the formation of the active Cu-Ni alloy.

SEM observations revealed irregular particle morphologies for all catalysts after impregnation (Figure 3). Furthermore, the average particle size distribution from SEM suggested that MSZ (Cu-Ni-WO_x/SiO_2-ZrO_2) catalyst showed the smallest particle size among the three catalysts, whereas the MZ (Cu-Ni-WO_x/ZrO_2) catalyst exhibited the largest particles. The MSZ and MS catalyst demonstrated relatively optimal metal dispersion due to the synergistic effect between SiO_2 and ZrO_2, in which the higher porosity of SiO_2 provided a larger accessible surface area for metal deposition [32-35], which is in line with the XRD results with the formation of Ni_2SiO_4 and the absence of Cu-Ni alloy.

EDX analysis confirmed the presence of the expected elements and indicated differences in metal distribution depending on the support (Table 2). The lower apparent concentration of metal species on SiO_2-containing supports may reflect broader dispersion over the support surface, while the ZrO_2-supported catalyst showed higher localized metal content. This result is in line with the XRD analysis that the crystal phase of *t*-ZrO_2 has lower elastic modulus than *m*-ZrO_2 leading to a more rigid structural framework that hinders uniform metal distribution within the support [35].

Figure 4A shows the acidity characteristics of the catalysts determined by pyridine-adsorbed FTIR. As presented in Figure 4B, the absorption bands at approximately 1544, 1484, and 1446 cm^{-1} correspond to Brønsted acid sites, the combined B+L acid sites, and Lewis acid sites, respectively. All catalysts exhibited these characteristic bands, indicating the coexistence of both Lewis and Brønsted acid sites on their surfaces.

The quantitative analysis of the acid sites shows that the MSZ (Cu-Ni-WO_x/SiO_2-ZrO_2) catalyst possesses the highest Lewis acidity (0.135 $mmol.g^{-1}$), followed by the B+L acid sites (0.065 $mmol.g^{-1}$) and Brønsted acidity (0.033

Table 1. Phase composition of catalysts obtained from Rietveld refinement of XRD data.

Phase	Phase Quantity (wt.%)		
	MSZ	MS	MZ
Cu°	0.92	1.33	2.73
Cu-Ni alloy	-	-	1.96
Ni_2SiO_4	12.85	11.66	-
WO_2	-	2.93	0.55
$WO_{2.72}$	3.85	2.91	1.28
SiO_2	26.49	81.17	-
t-ZrO_2	55.89	-	93.48
Weighted total	100.00	100.00	100.00

Table 2. Elemental composition of the catalyst surface determined by EDX analysis.

Catalyst	Type of metals and the quantities (wt.%)				
	Cu	Ni	W	Si	Zr
MSZ	7.7	5.75	3.84	12.56	19.78
MS	8.63	5.91	3.36	31.84	-
MZ	13.75	9.23	12.84	-	64.18

mmol g^{-1}). In comparison, the MS (Cu-Ni-WO_x/SiO_2) catalyst exhibits significantly lower amounts of all acid sites, while the MZ (Cu-Ni-WO_x/ZrO_2) catalyst shows moderate Lewis acidity but relatively higher B+L acidity than MS. Consequently, the total acidity (Figure 4C) follows the order MSZ > MZ > MS, confirming that the incorporation of both SiO_2 and ZrO_2 in the mixed support generates a larger number of accessible acid sites than the individual supports.

The enhanced acidity of the MSZ catalyst can be correlated with its phase composition. The MSZ catalyst consists of both amorphous SiO_2 and

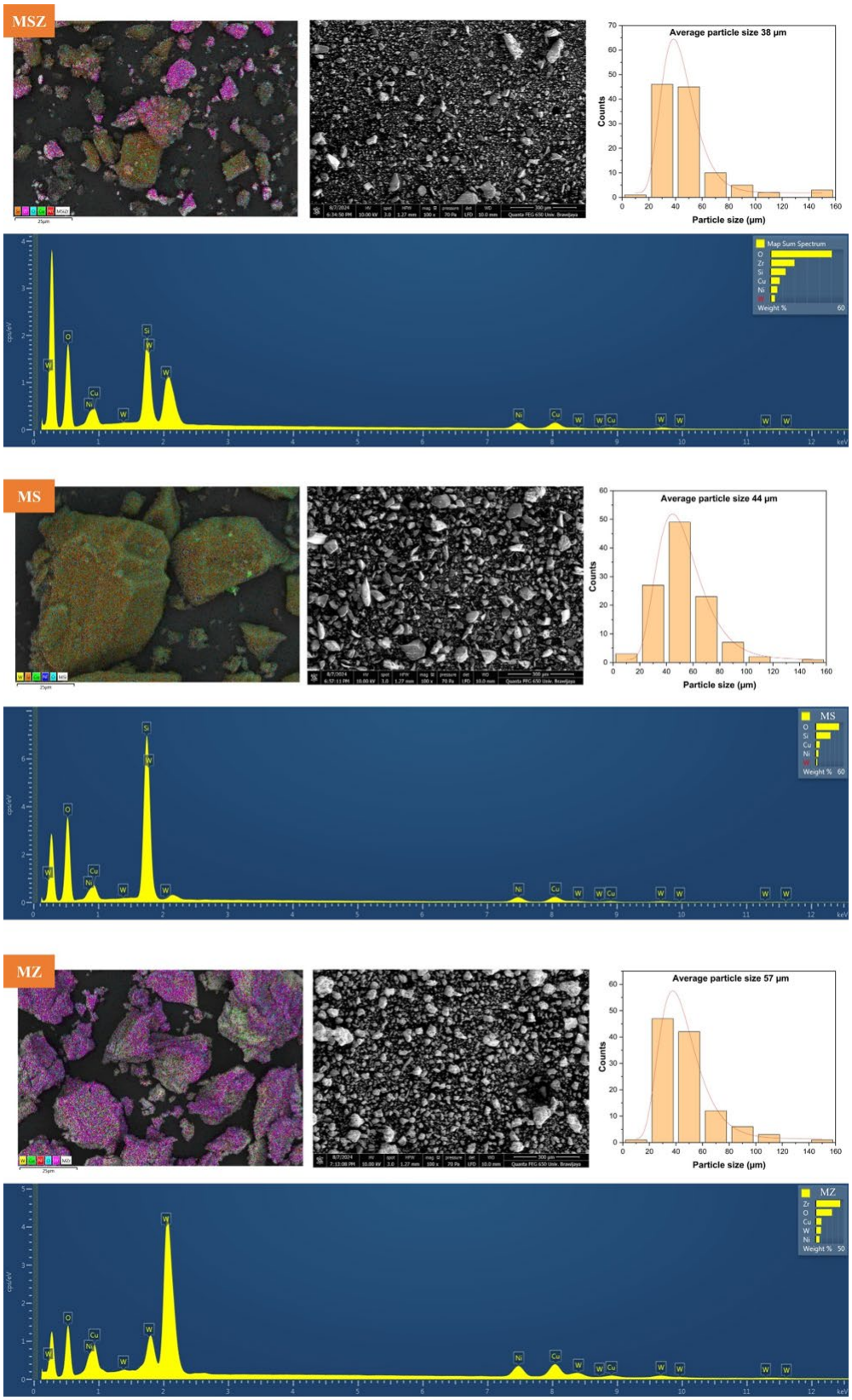

Figure 3. Catalyst characterization including SEM micrographs, EDX elemental spectra, and particle size distribution of the catalysts.

tetragonal ZrO_2, together with dispersed WO_x species ($WO_{2.72}$) and Ni_2SiO_4. The coexistence of SiO_2 and ZrO_2 is expected to generate interfacial Si–O–Zr linkages, which increase the number of coordinatively unsaturated Zr^{4+} species acting as Lewis acid sites, while tungsten oxide species further contribute to the formation of Brønsted acidity through surface W–OH groups [36] [37]. This synergistic interaction explains the substantially higher acidity observed for MSZ compared with the single-support catalysts.

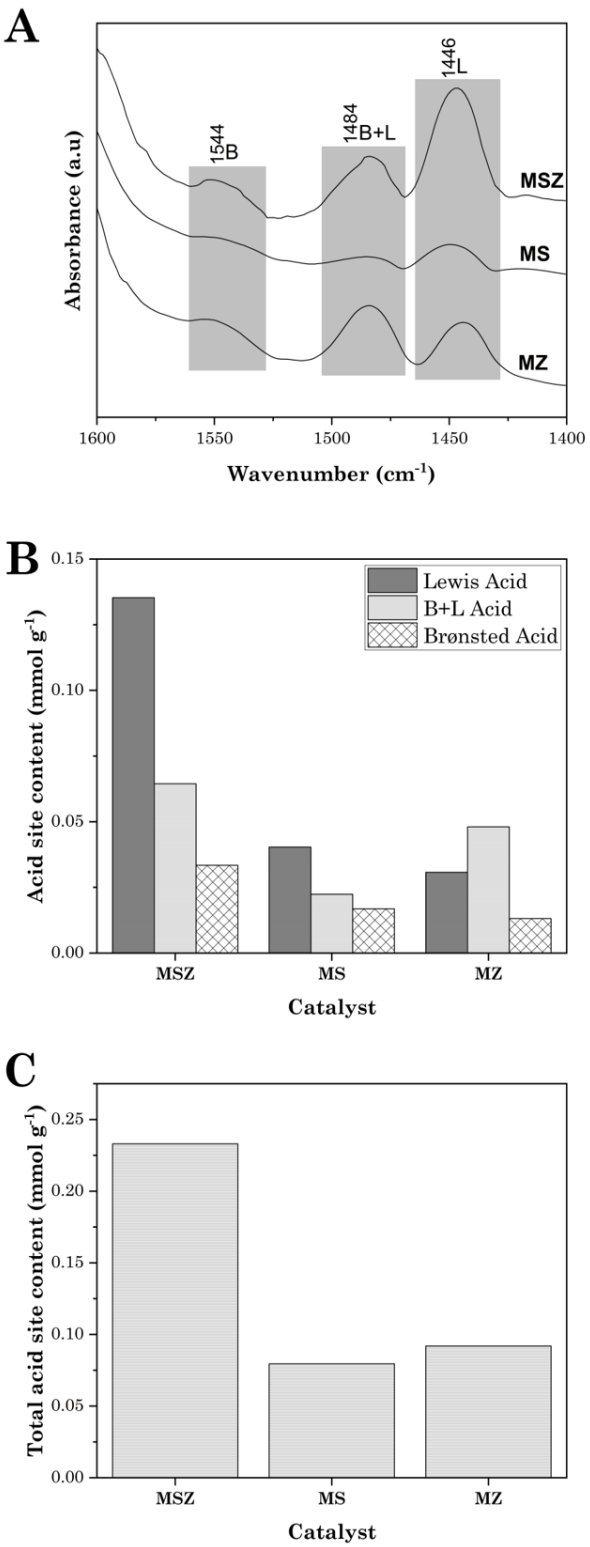

Figure 4. The Lewis acid sites and Brønsted acid sites of the catalysts: (A) FT-IR absorption spectra showing the interaction of pyridine with Lewis, Brønsted, and a combination of both acid sites (B+L); (B) distribution of acid site types on each catalyst; and (C) total catalyst acidity calculated based on the number of acid sites.

In contrast, the MS catalyst is dominated by amorphous SiO_2 provides a high surface area but intrinsically weak acidity. Although WO_2 and $WO_{2.72}$ phases are detected, the absence of ZrO_2 limits the formation of strong Lewis acid sites, resulting in the lowest total acidity among the catalysts. Concurrently, the MZ catalyst is predominantly composed of tetragonal ZrO_2, which contributes abundant Lewis acid centers through exposed Zr^{4+} ions. However, the absence of SiO_2 reduces the interfacial synergy responsible for generating additional acid sites, while the lower content of tungsten oxide species (1.83 wt.% total WO_x) restricts the development of Brønsted acidity [37]. As a result, its total acidity remains lower than that of MSZ despite its high ZrO_2 content.

3.2. Effect of Catalyst Support on Glucose Conversion

The catalytic hydrogenolysis of glucose over Cu-Ni-WO_x supported on different oxides (SiO_2-ZrO_2, SiO_2, and ZrO_2) revealed that the nature of the support plays a secondary role in total conversion but a dominant role in product selectivity. As depicted in Figure 5 that all catalysts exhibited comparable glucose conversion that is 92.2-93.1%, with no statistically significant difference ($p > 0.05$). This result suggests that the intrinsic activity of Cu-Ni active sites governs glucose conversion, while the support primarily influences downstream reaction pathways into product selectivity.

From a quantitative perspective, this behavior aligns with previous studies on Cu-based catalysts for glucose hydrogenolysis achieve conversion levels of 84-96% at 180-300 °C depending on hydrogen pressure and catalyst structure [38]. The other reported that Cu/γ-Al_2O_3 catalysts showed 100% conversion at 200 °C under similar hydrothermal conditions [39], which is highly consistent with the present system. Interestingly, although MSZ (Cu-Ni-WO_x/SiO_2-ZrO_2) exhibited higher acidity and smaller particle size, the highest conversion was observed over MZ (Cu-Ni-WO_x/ZrO_2). This indicates that the conversion is not directly proportional to total acidity or dispersion, but rather to the nature of active metal-support interfacial sites, especially those associated with WO_x-ZrO_2 interaction. This is supported by XRD observations showing sharper WO_x and solely support of t-ZrO_2 peaks for MZ creating Brønsted acid site higher, suggesting stronger crystallinity and potentially

more defined active sites. Similar findings were reported by Singha *et al.* and Yu *et al.*, where metal-support interaction strength influenced hydrogenolysis activity more than surface area or acidity alone [40,41].

3.2.1. Product distribution and control reaction

While the overall glucose conversion remained comparable across all catalysts, the product distribution exhibited significant variation, confirming that the nature of the catalyst support directing the reaction pathways. The liquid phase carbon balances were determined as 75.01% for MS (Cu-Ni-WO_x/SiO_2), 82.59% for MZ (Cu-Ni-WO_x/ZrO_2), and 80.17% for MSZ (Cu-Ni-WO_x/SiO_2-ZrO_2). The remaining carbon deficit (~17.41–24.99%) is ascribed to trace gaseous by-products as CO_2, light alkanes and insoluble humins typical of hydrothermal processing at 300 °C (Figure 5).

The SiO_2-supported catalyst MS (Cu-Ni-WO_x/SiO_2) produced the highest fraction of glycol and glycol-like compounds (40.87%), followed by MSZ (Cu-Ni-WO_x/SiO_2-ZrO_2) (26.52%) and MZ (Cu-Ni-WO_x/ZrO_2) (22.95%), indicating that weakly acidic supports favor pathways associated with C–C bond cleavage and retained the oxygen bond. This observation is consistent with recent studies reporting glycol yields in the range of 50-80% over catalysts dominated by retro-aldol mechanisms and subsequent hydrogenation steps [42]. Mechanistically, the relatively inert and weakly acidic nature of SiO_2 favors glucose isomerization to fructose, followed by retro-aldol cleavage into smaller intermediates such as glycolaldehyde, which are subsequently hydrogenated to short-chain polyols, including ethylene glycol and propylene glycol [43].

In parallel, the MS catalyst also exhibited the highest formation toward cyclic ether/THF derivatives (17.85%), significantly higher than MSZ (7.93%), which can be attributed to oxygen-retaining reaction pathways favored on weakly acidic supports. Recent studies have confirmed that silica-supported catalysts tend to preserve oxygenated functionalities and promote hydrogenation-cyclization sequences rather than deep deoxygenation, leading to THF derivatives with selectivity typically ranging from 10-25% [44,45]. This behavior reflects the limited ability of SiO_2 to activate C–O bonds, thereby suppressing rearrangement and hydrogenolysis pathways.

In contrast, the mixed oxide catalyst MSZ showed a markedly different selectivity profile, with the highest formation of cyclic ketones (31.53%) and a significant increase in aliphatic

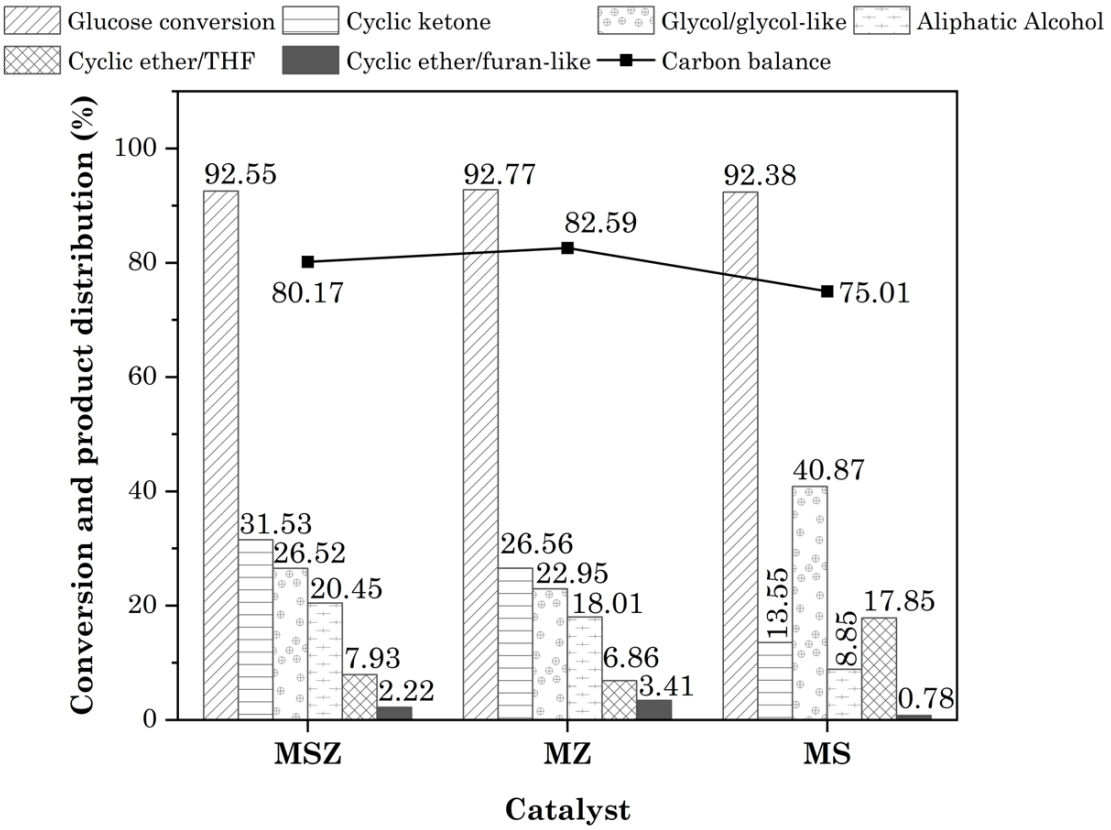

Figure 5. Conversion, product distribution, and carbon balance of liquids obtained from glucose hydrogenolysis over MSZ (Cu-Ni-WO_x/SiO_2-ZrO_2), MS (Cu-Ni-WO_x/SiO_2), and MZ (Cu-Ni-WO_x/ZrO_2) catalysts at 300 °C for 2 h under 2 MPa H_2 in water.

alcohols (20.45%) compared to MS and MZ. The cyclic ketone selectivity observed in this study falls within the upper range reported for bifunctional catalytic systems (20-40%), particularly those combining hydrogenation metals with Lewis acidic supports [45,46]. The formation of cyclic ketones is generally attributed to the Piancatelli-type rearrangement mechanism, which requires the synergistic effect between metal sites (Cu, Ni, and WO_x) as Lewis acid for hydrogenation and Brønsted acid sites (WO_x-ZrO_2) for carbonyl activation and rearrangement. The balanced acidity in the SiO_2-ZrO_2 support facilitates the formation of reactive intermediates and promotes their transformation into five-membered cyclic ketones, thereby enhancing selectivity [46].

Furthermore, the increased selectivity toward aliphatic alcohols over MSZ (20.45%) and MZ (18.01%) compared to MS highlights the role of zirconia-derived Lewis acidity in promoting C–O bond cleavage and hydrogenolysis reactions. Recent studies have shown that bifunctional catalysts consisting of transition metals and acidic supports can achieve alcohol yields in the range of 15-35%, depending on the distribution and strength of acid sites [47]. Stronger Lewis acidity enhances the polarization of carbonyl groups and facilitates bond cleavage, leading to the formation of linear alcohols through deoxygenation and fragmentation pathways [48].

Overall, these findings demonstrate that silica-based supports favor oxygen-retaining routes such as glycol and cyclic ether formation, whereas zirconia-containing supports promote deoxygenation, rearrangement, and hydrogenolysis pathways, resulting in higher selectivity toward cyclic ketones and aliphatic alcohols. The superior performance of the SiO_2-ZrO_2 mixed oxide catalyst highlights the importance of achieving an optimal balance between acidity and metal-support interaction to effectively control product distribution in glucose hydrogenolysis systems. The detailed the compound for each class is depicted in Scheme 1.

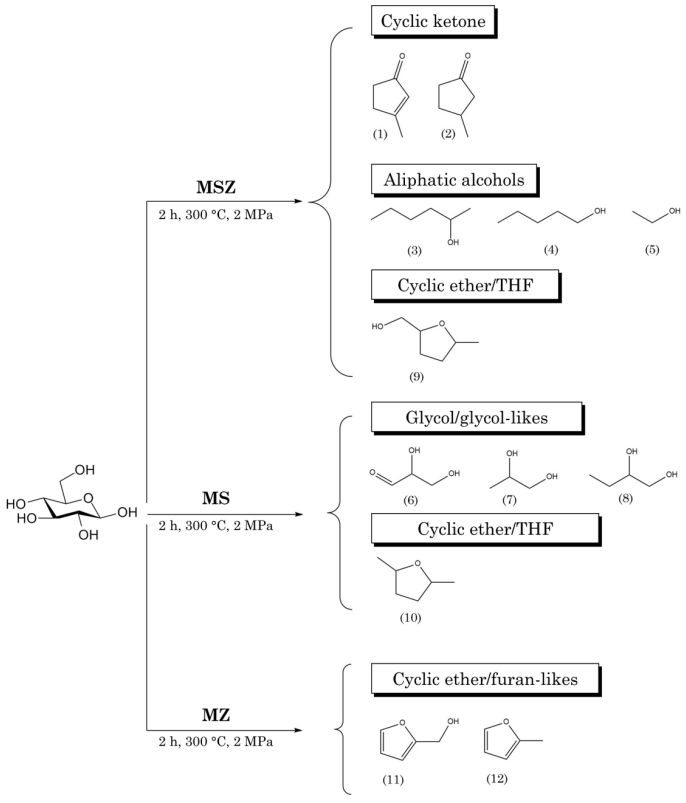

Scheme 1. Liquid product obtained from hydrogenolysis of glucose over MSZ (Cu-Ni-WO_x/SiO_2-ZrO_2), MS (Cu-Ni-WO_x/SiO_2), and MZ (Cu-Ni-WO_x/ZrO_2) catalysts, showing the preferential formation of cyclic ketones and aliphatic alcohols over silica/zirconia-containing catalysts and glycol-like/cyclic ether products over silica.

3.2.2. Plausible formation of cyclic ketones

The formation of cyclic ketones, such as cyclopentanone-type derivatives (Scheme 2), is commonly associated with the transformation of furanic intermediates through hydrogenation-rearrangement pathways [49]. In related biomass upgrading systems, such products are often generated via acid-assisted rearrangement of furfural- or HMF-derived intermediates, followed by hydrogenation of the resulting cyclic compounds [49]. The higher selectivity toward cyclic ketones over MSZ (Cu-Ni-WO_x/SiO_2-ZrO_2), and to a lesser extent over MZ (Cu-Ni-WO_x/ZrO_2), therefore suggests that zirconia-containing supports promoted reaction environments favorable for rearrangement pathway. The lower selectivity observed over MS (Cu-Ni-WO_x/SiO_2) indicates that silica alone was less effective in promoting this pathway. These results support the view that cyclic ketone formation in the present system was enhanced by support acidity, particularly when both hydrogenation-active metal sites and suitable acid sites were present.

3.2.3. Plausible formation of aliphatic alcohols

A plausible route to aliphatic alcohol formation involves competition between oxygen-retaining pathways and deoxygenation-rearrangement pathways (Scheme 3). In biomass conversion systems, sugar-derived or furan-derived intermediates may undergo hydrogenation, hydrogenolysis, and hydrodeoxygenation steps to yield shorter-chain alcohols and related oxygenates [50,51]. In the present study, the higher fraction of aliphatic alcohols obtained over MSZ (Cu-Ni-WO_x/SiO_2-ZrO_2) suggests that the balanced acidity of the mixed-oxide support promoted hydrogenolysis

and ring-opening reactions more effectively than the silica-supported catalyst. In contrast, the lower selectivity toward aliphatic alcohols over MS (Cu-Ni-WO_x/SiO_2) is consistent with a catalyst environment that tends to preserve oxygenated structures rather than promote further transformation. Thus, the formation of aliphatic alcohols appears to be favored by catalysts that combine appropriate metal functionality with a more suitable Lewis-Brønsted acidity balance.

3.2.4. Plausible formation of glycol/glycol-like compounds

The formation of glycol/glycol-like compounds is commonly associated with pathways involving isomerization, retro-aldol cleavage, and subsequent hydrogenation of smaller oxygenated intermediates [52,53], as shown in Scheme 4. Selective C–C and C–O bond cleavage strategies are particularly important for generating short-chain polyols and related compounds from carbohydrate-derived substrates [52]. The much higher fraction of glycol/glycol-like compounds observed over MS (Cu-Ni-WO_x/SiO_2) suggests that the silica-supported catalyst favored these oxygen-retaining cleavage pathways without driving the intermediates further toward rearranged cyclic products or deeper deoxygenation. By contrast, the lower glycol selectivity over MZ (Cu-Ni-WO_x/ZrO_2) and MSZ (Cu-Ni-WO_x/SiO_2-ZrO_2) indicates that zirconia-containing supports promoted competing reaction routes, including rearrangement and hydrogenolysis, thereby decreasing the relative accumulation of glycol-like products.

3.2.5. Plausible formation of cyclic ether/THF and cyclic ether/furan-like

The formation of cyclic ether/THF compounds is consistent with reaction networks involving hydrogenation and cyclization of furanic intermediates (Scheme 5). In related biomass upgrading systems, HMF and BHMF-type intermediates may be further hydrogenated to THF-based products under catalyst environments that preserve oxygenated ring structures [54,55]. Such transformations are also closely related to the broader catalytic chemistry of carbohydrate-derived furan compounds and their hydrogenation products [56,57]. The

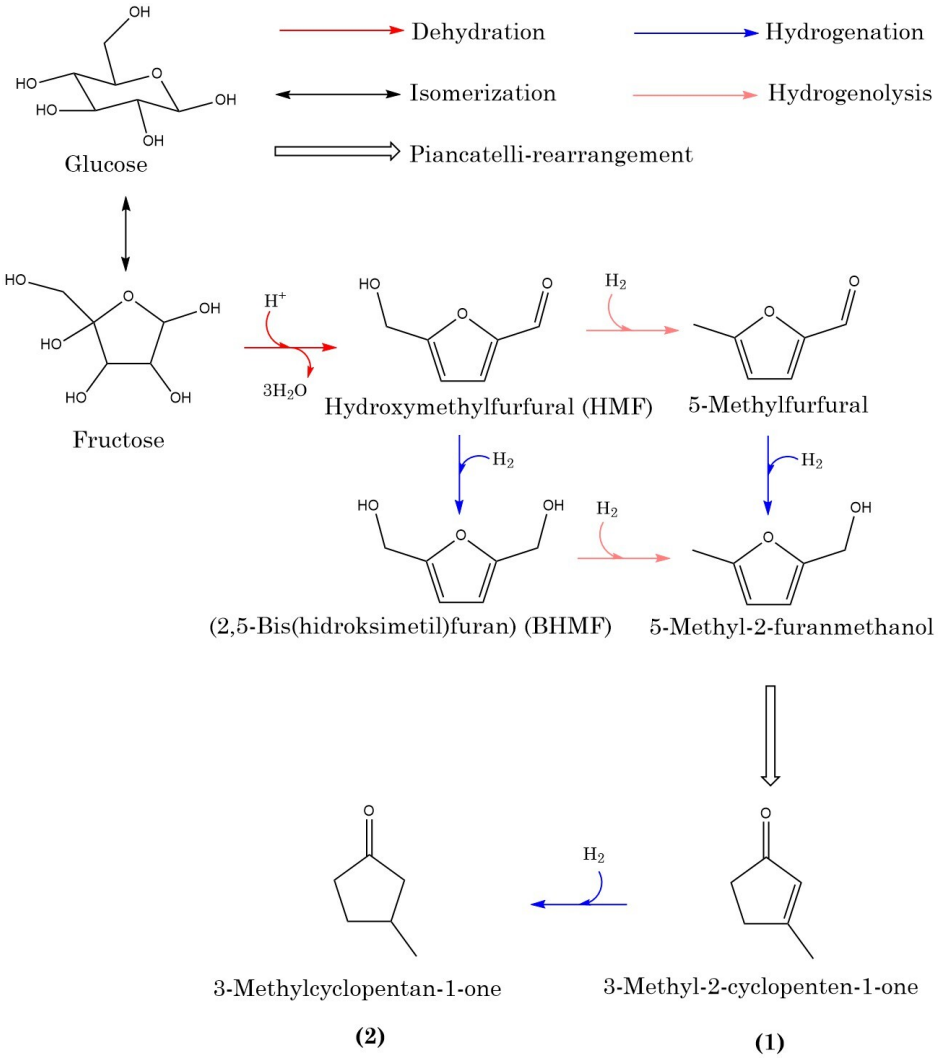

Scheme 2. Reaction pathways for the catalytic conversion of glucose into cyclic ketone.

relatively high selectivity toward cyclic ether/THF products over MS (Cu-Ni-WO_x/SiO_2) suggests that the silica-supported catalyst favored hydrogenation and oxygen-retaining cyclization pathways without strongly promoting rearrangement or extensive C-O bond cleavage. In contrast, the lower fraction of cyclic ether/THF products over MSZ (Cu-Ni-WO_x/SiO_2-ZrO_2) and MZ (Cu-Ni-WO_x/ZrO_2) indicates that zirconia-containing supports shifted the reaction network toward competing pathways, including ketone and alcohol formation.

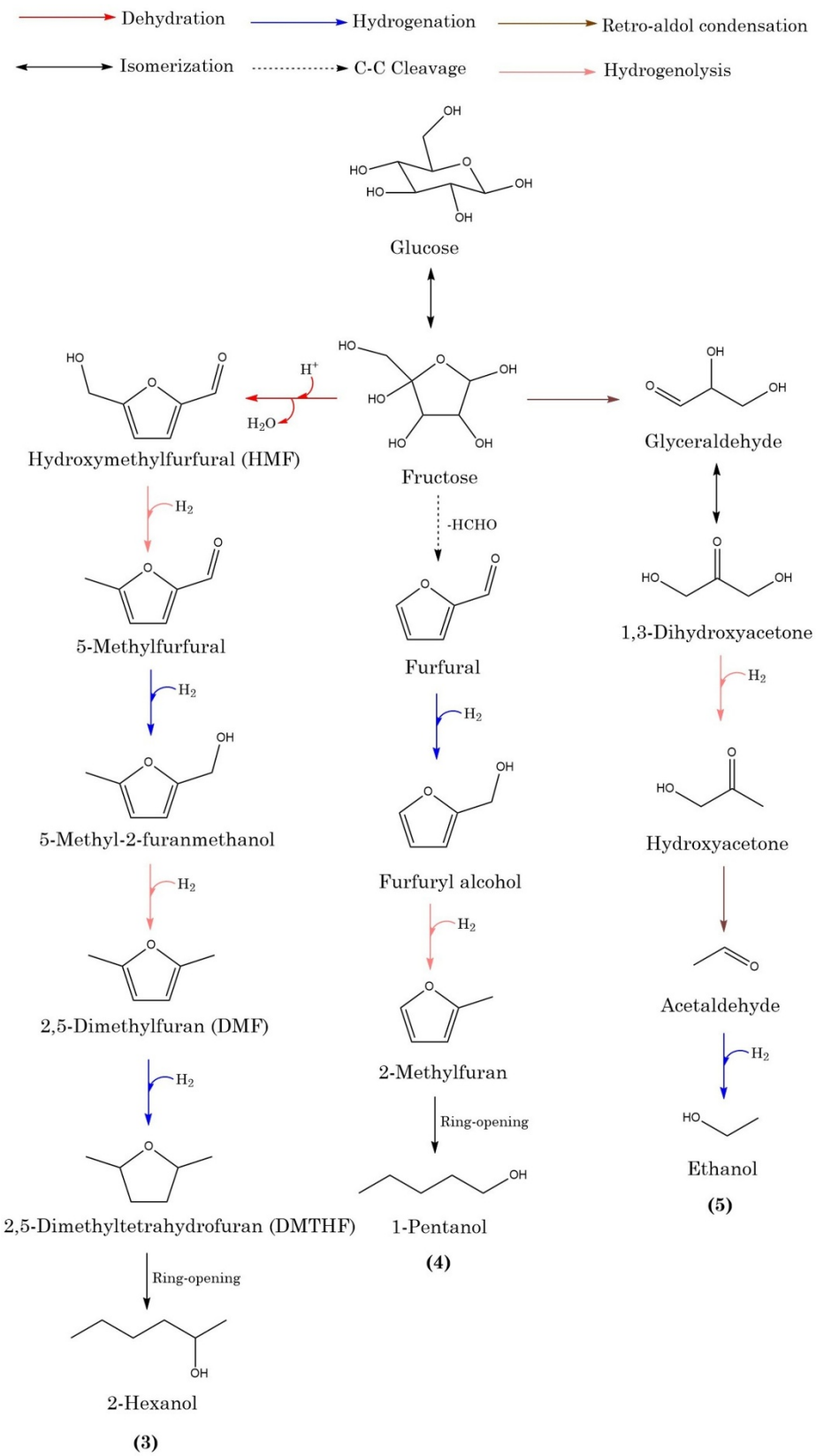

Scheme 3. Reaction pathways for the catalytic conversion of glucose into aliphatic alcohols.

The formation of cyclic ether/furan-like products over MZ (Cu-Ni-WO_x/ZrO_2) and MSZ (Cu-Ni-WO_x/SiO_2-ZrO_2) may likewise reflect a more reactive catalytic environment in which furan-derived intermediates undergo partial hydrogenation and parallel side transformations (Scheme 6). Although these products were present only in minor amounts, their appearance supports the view that support composition influenced the branching of the glucose hydrogenolysis network.

4. Conclusions

The Cu-Ni-WO_x catalysts supported on SiO_2, ZrO_2, and SiO_2-ZrO_2 showed comparable glucose conversion under the studied reaction conditions, but markedly different liquid product distributions. The SiO_2-supported catalyst, which was predominantly composed of amorphous SiO_2, favored the formation of oxygen-retaining products, particularly glycol/glycol-like compounds and cyclic ether/THF derivatives. In contrast, the mixed SiO_2-ZrO_2-supported catalyst, consisting of both amorphous SiO_2 and tetragonal ZrO_2 together with dispersed WO_x species, exhibited higher selectivity toward cyclic ketones and aliphatic alcohols. However, the ZrO_2-supported catalyst, dominated by tetragonal ZrO_2, displayed an intermediate selectivity pattern. These differences demonstrate that the support-dependent phase distribution influences the acidity profile and, consequently, the reaction pathways during

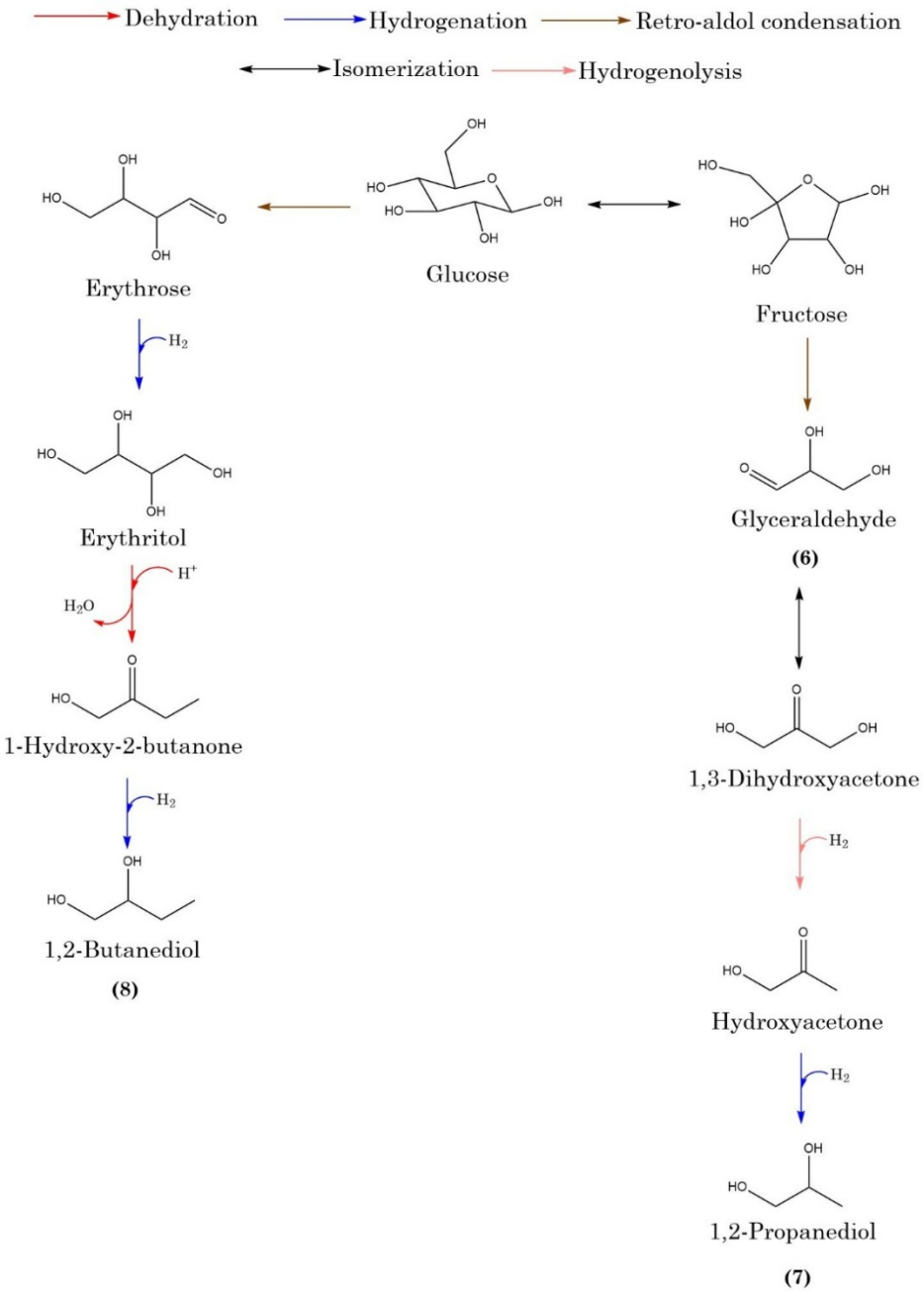

Scheme 4. Reaction pathways for the catalytic conversion of glucose into glycol/glycol-likes.

glucose hydrogenolysis over Cu-Ni-WO_x catalysts. In particular, the synergistic coexistence of SiO_2 and ZrO_2 phases in the mixed-oxide support generated a more favorable catalytic environment, characterized by enhanced acidity, which promoted product formation through rearrangement and hydrogenolysis rather than oxygen-retaining pathways. This study provides valuable insight into how tailoring the phase composition and acidity of single-oxide and mixed-oxide supports can be used to control the selectivity of Cu-Ni-WO_x catalysts for biomass-derived glucose conversion.

Acknowledgment

This work was supported by the Magister Thesis Research Grant (PTM), Ministry of Higher Education, Indonesia, No. 00309.92/UN10.A0501/B/PT.01.03.2/2024, and in part by a research grant from the Faculty of Science, No. 07629.32/UN10.F0901/B/PT/2025. The authors also gratefully thank the Central Laboratory of Brawijaya University (LRT) for access to XRD and FESEM instrumentation.

CRedit Author Statement

Author Contributions: Conceptualization: Siti Mariyah Ulfa, Yuniar Ponco Prananto, Ahmad Sholeh Romdlon; Methodology: Ahmad Sholeh Romdlon, Siti Mariyah Ulfa, Yuniar Ponco Prananto; Investigation: Ahmad Sholeh Romdlon; Data curation: Ahmad Sholeh Romdlon; Formal analysis: Ahmad Sholeh Romdlon, Yuniar Ponco Prananto; Writing – original draft: Ahmad Sholeh Romdlon; Writing – review & editing: Siti Mariyah Ulfa, Yuniar Ponco Prananto, Ahmad Sholeh Romdlon; Supervision: Siti Mariyah Ulfa, Yuniar Ponco

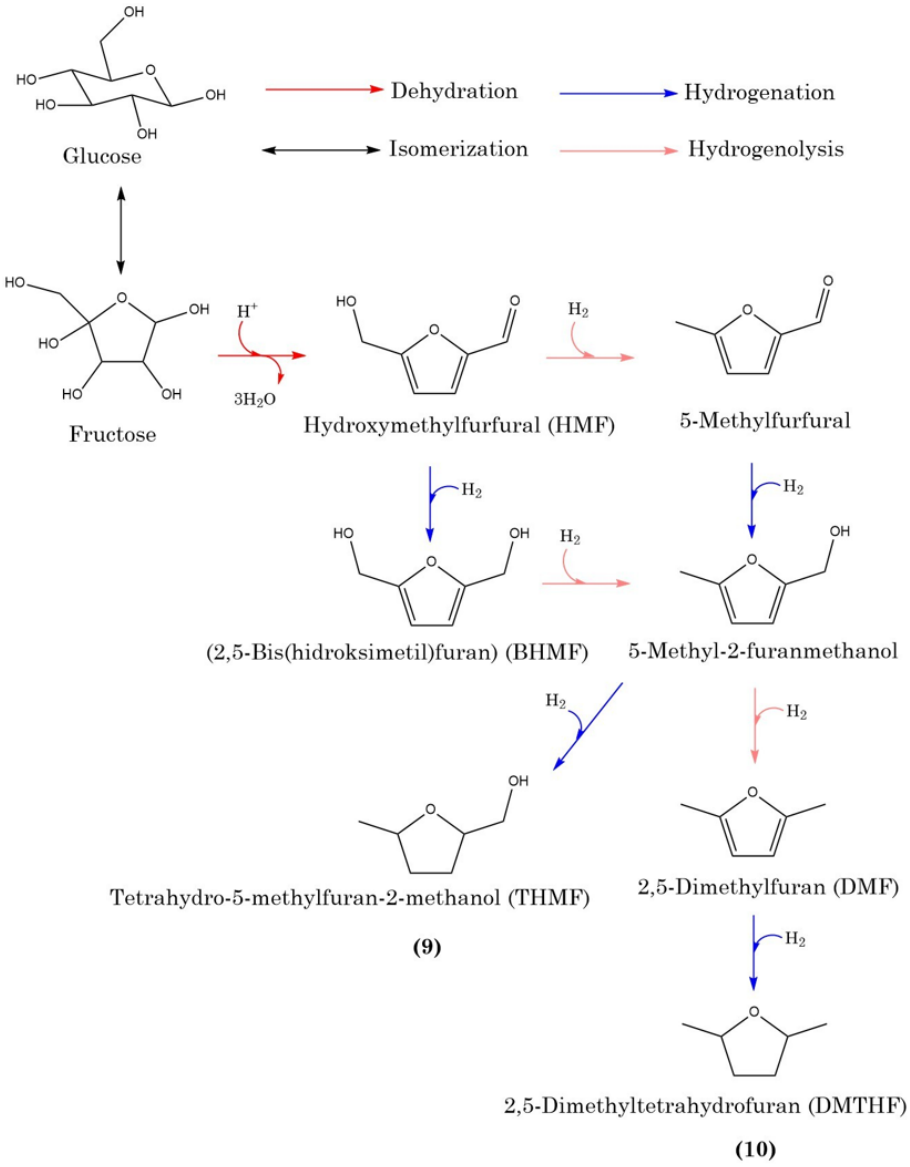

Scheme 5. Reaction pathways for the catalytic conversion of glucose into cyclic ether/THF.

Prananto. All authors have read and agreed to the published version of the manuscript.

Notes for Usage of Generative AI in Scientific Writing

The authors declare that generative AI and AI-assisted technologies were used solely for the purpose of improving the clarity, readability, and language of this manuscript. All outputs generated by these tools were carefully reviewed, edited, and validated by the authors. The authors take full responsibility for the content of this work.

References

[1] Azzahra, A.S., Dewi, H.P., Mikrianto, E., Sembiring, K.C., Sunnardianto, G.K., Nata, I.F., Rodiansono, R., Jayanudin, J. (2023). Bimetallic Ru-Sn as Effective Catalysts for the Selective Hydrogenation of Biogenic Platform Chemicals at Room Temperature. *Bulletin of Chemical Reaction Engineering & Catalysis*, 18(4), 700–712. DOI: 10.9767/bcrec.20067.

[2] Damayanti, D., Wulandari, Y.R., Wu, H.-S. (2020). Product Distribution of Chemical Product Using Catalytic Depolymerization of Lignin. *Bulletin of Chemical Reaction Engineering & Catalysis*, 15(2), 432–453. DOI: 10.9767/bcrec.15.2.7249.432-453.

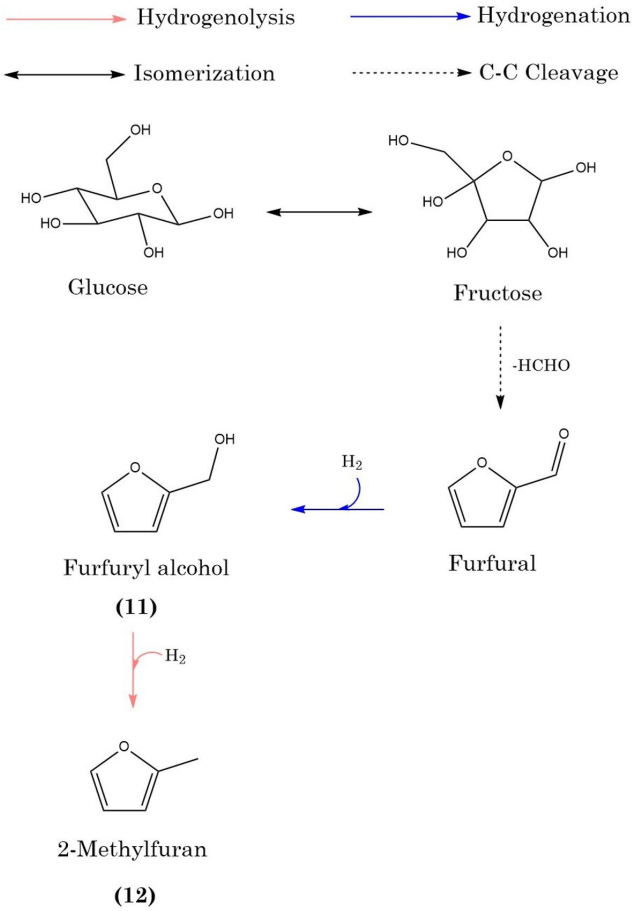

Scheme 6. Reaction pathways for the catalytic conversion of glucose into cyclic ether/furan-

[3] Baniamerian, H., Høj, M., Beier, M.J., Jensen, A.D. (2023). Catalytic conversion of sugars and polysaccharides to glycols: A review. *Applied Catalysis B: Environmental*, 330, 122650. DOI: 10.1016/j.apcatb.2023.122650.

[4] Akhtar, M.S., Naseem, M.T., Ali, S., Zaman, W. (2025). Metal-Based Catalysts in Biomass Transformation: From Plant Feedstocks to Renewable Fuels and Chemicals. *Catalysts*, 15(1). DOI: 10.3390/catal15010040

[5] Chávez-Sifontes, M., Ventura, M. (2024). Metal-Based Heterogeneous Catalysts for the Synthesis of Valuable Chemical Blends via Hydrodeoxygenation of Lignin-Derived Fractions. *Catalysts*, 14(2). DOI: 10.3390/catal14020146

[6] Fung, V., Janik, M., Crossley, S., Chin, Y.-H.C., Savara, A. (2023). Toward Understanding and Controlling Organic Reactions on Metal Oxide Catalysts. *The Journal of Physical Chemistry C*, 127(28), 13451–13465. DOI: 10.1021/acs.jpcc.3c02470

[7] Hagen, J. (2006). *Industrial Catalysis: A Practical Approach* (2nd ed.). Die Deutsche Bibliothek.

[8] Dagle, V.L., Flake, M.D., Lemmon, T.L., Lopez, J.S., Kovarik, L., Dagle, R.A. (2018). Effect of the SiO2 support on the catalytic performance of Ag/ZrO2/SiO2 catalysts for the single-bed production of butadiene from ethanol. *Applied Catalysis B: Environmental*, 236, 576–587. DOI: 10.1016/j.apcatb.2018.05.055

[9] Deshmane, V., Adewuyi, Y.G. (2012). Synthesis of Thermally Stable, High Surface Area, Nanocrystalline Mesoporous Tetragonal Zirconium Dioxide (ZrO2): Effects of Different Process Parameters. *Microporous and Mesoporous Materials*, 148(1), 88–100. DOI: 10.1016/j.micromeso.2011.07.012

[10] Zhang, W., Zhu, Y., Xu, H., Gaborieau, M., Huang, J., Jiang, Y. (2020). Glucose conversion to 5-hydroxymethylfurfural on zirconia: Tuning surface sites by calcination temperatures. *Sydney Catal. Symposium,* 18, 351, 133–140. DOI: 10.1016/j.cattod.2018.10.002

[11] Wang, Y., Wang, H., Kong, X., Zhu, Y. (2022). Catalytic Conversion of 5-Hydroxymethylfurfural to High-Value Derivatives by Selective Activation of C–O, C=O, and C=C Bonds. *ChemSusChem*, 15(13), e202200421. DOI: 10.1002/cssc.202200421

[12] Wang, Q., Yu, Z., Feng, J., Fornasiero, P., He, Y., Li, D. (2020). Insight into the Effect of Dual Active Cu0/Cu+ Sites in a Cu/ZnO-Al2O3 Catalyst on 5-Hydroxylmethylfurfural Hydrodeoxygenation. *ACS Sustainable Chemistry & Engineering*, 8(40), 15288–15298. DOI: 10.1021/acssuschemeng.0c05235

[13] Zhu, Y., Kong, X., Peng, B., Li, L., Fang, Z., Zhu, Y. (2020). Efficient Cu catalyst for 5-hydroxymethylfurfural hydrogenolysis by forming Cu–O–Si bonds. *Catalysis Science & Technology*, 10(21), 7323–7330. DOI: 10.1039/D0CY01032D

[14] Liao, X., Zhao, H., Liu, R., Luo, H., Lv, Y., Liu, P. (2024). Highly efficient and selective hydrogenation of furfural to furfuryl alcohol and cyclopentanone over Cu-Ni bimetallic Catalysts: The crucial role of CuNi alloys and Cu+ species. *Journal of Catalysis*, 436, 115603. DOI: 10.1016/j.jcat.2024.115603

[15] Astuti, M.D., Kristina, D., Rodiansono, R., Mujiyanti, D.R. (2020). One-pot Selective Conversion of Biomass-derived Furfural into Cyclopentanone/Cyclopentanol over TiO2 Supported Bimetallic Ni-M (M = Co, Fe) Catalysts. *Bulletin of Chemical Reaction Engineering & Catalysis,* 15(1), 231–241. DOI: 10.9767/bcrec.15.1.6307.231-241

[16] Ahmed, S., Abdullah, I., Krisnandi, Y.K. (2025). Harnessing Copper's Potential: A Review of Cu-Based Catalysts for Glycerol Conversion. *Bulletin of Chemical Reaction Engineering & Catalysis*, 20(2), 193–220. DOI: 10.9767/bcrec.20341

[17] Huang, W., Xu, Q., Lu, H., Yao, X., Ye, Y., Zhou, R., Li, D., Ye, T. (2025). Non-precious Cu/WO3 catalyst for hydrogenolysis of HMF to 5-MF with ultra-high selectivity in a continuous flow reactor. *New Journal of Chemistry*, 49(11), 4400–4409. DOI: 10.1039/D5NJ00160A

[18] Qiao, Y., Xia, G.-J., Cao, W., Zeng, K.-H., Guo, Q.-L., Yang, X.-F., Wang, A.-Q., Wang, Y.-G. (2023). Breaking the C–C bond of glucose on tungsten oxide-based catalysts in aqueous phase. *Journal of Catalysis*, 427, 115114. DOI: 10.1016/j.jcat.2023.115114

[19] Sowe, M.S., Lestari, A.R., Novitasari, E., Masruri, M., Ulfa, S.M. (2022). The Production of Green Diesel Rich Pentadecane (C15) from Catalytic Hydrodeoxygenation of Waste Cooking Oil using Ni/Al2O3-ZrO2 and Ni/SiO2-ZrO2. *Bulletin of Chemical Reaction Engineering & Catalysis*, 17(1), 135–145. DOI: 10.9767/bcrec.17.1.12700.135-145

[20] Ulfa, S.M., Munandar, R., Prihartini, D. (2018). Batch and continuous flow hydrodeoxygenation of furfural and acetone condensation adduct catalyzed by Ni/ZrO2-SiO2. *AIP Conference Proceedings*, 2049(1), 020005. DOI: 10.1063/1.5082410

[21] Yu, J., Liang, J., Chen, X., Wang, L., Wei, X., Li, Y., Qin, Y. (2021). Synergistic Effect of Ni/W/Cu on MgAl2O4 for One-Pot Hydrogenolysis of Cellulose to Ethylene Glycol at a Low H2 Pressure. *ACS Omega*, 6(17), 11650–11659. DOI: 10.1021/acsomega.1c00979

[22] Romdlon, A.S., Fadana, Y., Marno, S., Ulfa, S.M. (2024). The production of bioethanol from ethylene glycol as renewable energy using Ni-Cu based catalyst. *AIP Conference Proceedings*, 3055(1), 050001. DOI: 10.1063/5.0193615

[23] Hartati, H., A'yuni, Q., Dewi, N.S., Firda, P.B.D., Izzah, A.N., Prasetyoko, D., Harmami, H., Ahmad, S.N. (2024). Synthesis and Characterization of Aluminosilicate Catalysts from Volcano Mud for Biofuel Production with Different Feedstocks. *Indonesian Journal of Chemistry,* 24(6). DOI: 10.22146/Ijc.96149.

[24] Emeis, C.A. (1993). Determination of Integrated Molar Extinction Coefficients for Infrared Absorption Bands of Pyridine Adsorbed on Solid Acid Catalysts. *Journal of Catalysis*, 141(2), 347–354. DOI: 10.1006/jcat.1993.1145

[25] Wu, W., Weitz, E. (2014). Modification of acid sites in ZSM-5 by ion-exchange: An in-situ FTIR study. *Applied Surface Science*, 316, 405–415. DOI: 10.1016/j.apsusc.2014.07.194

[26] Krivorotova, T., Sereikaite, J. (2014). Determination of fructan exohydrolase activity in the crude extracts of plants. *Electronic Journal of Biotechnology*, 17(6), 329–333. DOI: 10.1016/j.ejbt.2014.09.005

[27] Natile, M.M., Galenda, A., Glisenti, A., Mascotto, S., Gross, S. (2009). Silica–zirconia mixed oxide samples by an hybrid materials based innovative preparation procedure: Influence of preparation procedure and composition on active sites. *Journal of Non-Crystalline Solids*, 355(8), 481–487. DOI: 10.1016/j.jnoncrysol.2009.01.021

[28] Pyen, S., Hong, E., Shin, M., Suh, Y.-W., Shin, C.-H. (2018). Acidity of co-precipitated SiO2-ZrO2 mixed oxides in the acid-catalyzed dehydrations of iso-propanol and formic acid. *Molecular Catalysis*, 448, 71–77. DOI: 10.1016/j.mcat.2018.01.031

[29] Ren, H., Cheng, J., Fang, H., Zhong, F., Chen, C., Lin, L., Luo, Y., Au, C., Jiang, L., Lin, X. (2023). Phyllosilicate-derived Ni catalysts with small nanoparticle size and strong metal-support interaction for efficient and robust decomposition of ammonia. *Applied Catalysis A: General*, 664, 119344. DOI: 10.1016/j.apcata.2023.119344

[30] Wang, K., Men, Y., Liu, S., Wang, J., Li, Y., Tang, Y., Li, Z., An, W., Pan, X., Li, L. (2021). Decoupling the size and support/metal loadings effect of Ni/SiO2 catalysts for CO2 methanation. *Fuel*, 304, 121388. DOI: 10.1016/j.fuel.2021.121388

[31] Wang, J., Zhao, X., Lei, N., Li, L., Zhang, L., Xu, S., Miao, S., Pan, X., Wang, A., Zhang, T. (2016). Hydrogenolysis of Glycerol to 1,3-propanediol under Low Hydrogen Pressure over WOx-Supported Single/Pseudo-Single Atom Pt Catalyst. *ChemSusChem*, 9(8), 784–790. DOI: 10.1002/cssc.201501506

[32] Chen, C., Wang, W., Ren, Q., Ye, R., Nie, N., Liu, Z., Zhang, L., Xiao, J. (2022). Impact of preparation method on nickel speciation and methane dry reforming performance of Ni/SiO2 catalysts. *Frontiers in Chemistry*, 10. DOI: 10.3389/fchem.2022.993691

[33] Zhang, X., Zhang, Q., Chen, L., Xu, Y., Wang, T., Ma, L. (2014). Effect of calcination temperature of Ni/SiO2-ZrO2 catalyst on its hydrodeoxygenation of guaiacol. *Chinese Journal of Catalysis*, 35(3), 302–309. DOI: 10.1016/S1872-2067(12)60733-5

[34] Rad, A.R.S., Khoshgouei, M.B., Rezvani, S., Rezvani, A.R. (2012). Study of Cu–Ni/SiO2 catalyst prepared from a novel precursor, [Cu(H2O)6][Ni(dipic)2].2H2O/SiO2, for water gas shift reaction. *Fuel Processing Technology*, 96, 9–15. DOI: 10.1016/j.fuproc.2011.12.015

[35] Liang, Z., Wang, W., Zhang, M., Wu, F., Chen, J.-F., Xue, C., Zhao, H. (2017). Structural, mechanical and thermodynamic properties of ZrO2 polymorphs by first-principles calculation. *Physica B: Condensed Matter*, 511, 10–19. DOI: 10.1016/j.physb.2017.01.025

[36] Zhou, W., Soultanidis, N., Xu, H., Wong, M.S., Neurock, M., Kiely, C.J., Wachs, I.E. (2017). Nature of Catalytically Active Sites in the Supported WO3/ZrO2 Solid Acid System: A Current Perspective. *ACS Catalysis*, 7(3), 2181–2198. DOI: 10.1021/acscatal.6b03697

[37] Zhang, W., Wang, Z., Marianov, A., Zhu, Y., Wang, L., Castignolles, P., Gaborieau, M., Baiker, A., Huang, J., Jiang, Y. (2025). Boosting the Formation of Brønsted Acids on Flame-made WOx/ZrO2 for Glucose Conversion. *ChemSusChem*, 18(1), e202400128. DOI: 10.1002/cssc.202400128

[38] Sebastian, J., Zheng, M., Li, X., Pang, J., Wang, C., Zhang, T. (2019). Catalytic conversion of glucose to small polyols over a binary catalyst of vanadium modified beta zeolite and Ru/C. *Journal of Energy Chemistry*, 34, 88–95. DOI: 10.1016/j.jechem.2018.10.003

[39] Balachandran Kirali, A.A., Sreekantan, S., Marimuthu, B. (2022). Ce promoted Cu/γ-Al2O3 catalysts for the enhanced selectivity of 1,2-propanediol from catalytic hydrogenolysis of glucose. *Catalysis Communications*, 165, 106447. DOI: 10.1016/j.catcom.2022.106447

[40] Singha, R.K., Shukla, A., Yadav, A., Sivakumar Konathala, L.N., Bal, R. (2017). Effect of metal-support interaction on activity and stability of Ni-CeO2 catalyst for partial oxidation of methane. *Applied Catalysis B: Environmental*, 202, 473–488. DOI: 10.1016/j.apcatb.2016.09.060

[41] Yu, X., Zhang, J., Yang, H., Chong, S., Liu, G., Zhang, Y., Wang, K. (2024). Effect of the metal-support interaction in the Cu/ZnO catalyst on its performance in the hydrogenation of furfural to furfuryl alcohol. *Journal of Fuel Chemistry and Technology*, 52(8), 1045–1056. DOI: 10.1016/S1872-5813(24)60445-7

[42] Pang, J., Zheng, M., Li, X., Jiang, Y., Zhao, Y., Wang, A., Wang, J., Wang, X., Zhang, T. (2018). Selective conversion of concentrated glucose to 1,2-propylene glycol and ethylene glycol by using RuSn/AC catalysts. *Applied Catalysis B: Environmental*, 239, 300–308. DOI: 10.1016/j.apcatb.2018.08.022

[43] Song, J., Wang, D., Wang, Q., Cui, C., Yang, Y. (2024). Selective Control of Catalysts for Glycerol and Cellulose Hydrogenolysis to Produce Ethylene Glycol and 1,2-Propylene Glycol: A Review. *Catalysts*, 14(10), 685. DOI: 10.3390/catal14100685

[44] Chimentão, R.J., Oliva, H., Belmar, J., Morales, K., Mäki-Arvela, P., Wärnå, J., Murzin, D. Yu., Fierro, J.L.G., Llorca, J., Ruiz, D. (2019). Selective hydrodeoxygenation of biomass derived 5-hydroxymethylfurfural over silica supported iridium catalysts. *Applied Catalysis B: Environmental*, 241, 270–283. DOI: 10.1016/j.apcatb.2018.09.026

[45] Serrano-Ruiz, J.C., Dumesic, J.A. (2011). Catalytic routes for the conversion of biomass into liquid hydrocarbon transportation fuels. *Energy & Environmental Science*, 4(1), 83–99. DOI: 10.1039/C0EE00436G

[46] van Slagmaat, C.A.M.R. (2025). The Cascade Transformation of Furfural to Cyclopentanone: A Critical Evaluation Concerning Feasible Process Development. *ChemEngineering*, 9(4), 74. DOI: 0.3390/chemengineering9040074

[47] Mokwena, H.P., Beas, I.N., Li, H., Nyangiwe, N.N., Bingwa, N. (2025). Towards attainment of value-added chemicals with industrial applications over versatile LaCo1-xMnxO3±δ perovskites: In-depth computational interrogation of catalyst properties. *Sustainable Materials and Technologies*, 45, e01517. DOI: 10.1016/j.susmat.2025.e01517

[48] Jiang, Z., Zeng, Y., Hu, D., Guo, R., Yan, K., Luque, R. (2023). Chemical transformations of 5-hydroxymethylfurfural into highly added value products: Present and future. *Green Chemistry*, 25(3), 871–892. DOI: 10.1039/D2GC03444A

[49] Duan, Y., Cheng, Y., Hu, Z., Wang, C., Sui, D., Yang, Y., Lu, T. (2023). A Comprehensive Review on Metal Catalysts for the Production of Cyclopentanone Derivatives from Furfural and HMF. *Molecules*, 28(14), 5397. DOI: 10.3390/molecules28145397

[50] Xia, Q., Chen, Z., Shao, Y., Gong, X., Wang, H., Liu, X., Parker, S.F., Han, X., Yang, S., Wang, Y. (2016). Direct hydrodeoxygenation of raw woody biomass into liquid alkanes. *Nature Communications*, 7(1), 11162. DOI: 10.1038/ncomms11162

[51] Tong, X., Ma, Y., Li, Y. (2010). Biomass into chemicals: Conversion of sugars to furan derivatives by catalytic processes. *Applied Catalysis A: General*, 385(1), 1–13. DOI: 10.1016/j.apcata.2010.06.049

[52] Sun, R., Yang, C., Fang, Z., Zhu, N., Zheng, M., Guo, K., Zhang, T. (2024). Selective C–C and C–O bond cleavage strategies for the thermochemical upgrading of (hemi)cellulosic biomass. *Applied Catalysis B: Environment and Energy*, 344, 123599. DOI: 10.1016/j.apcatb.2023.123599

[53] Zhang, L., Huang, S., Qiu, J., Wang, B., Yan, B., Zhang, J., Zhou, B., Chen, J., Zeng, X. (2023). Selective transformation of biomass-derived substrates to 1,2-butanediol: A comprehensive review and new insights. *Industrial Crops and Products*, 202, 116984. DOI: 10.1016/j.indcrop.2023.116984

[54] Achour, A., Ojagh, H., Ho, P.H., Creaser, D., Pajalic, O., Holmberg, J., Olsson, L. (2023). Towards stable nickel catalysts for selective hydrogenation of biomass-based BHMF into THFDM. *Journal of Environmental Chemical Engineering*, 11(2), 109461. DOI: 10.1016/j.jece.2023.109461

[55] Zhu, X., Wang, F., Yang, L., Chen, Z., Zhao, K., Liu, X., Xu, Q., Yin, D., Yu, N. (2024). Silica-supported non-precious copper catalyst for catalytic hydrogenation of 5-hydroxymethylfurfural to 2,5-bis(hydroxymethyl)furan. *Molecular Catalysis*, 553, 113794. DOI: 10.1016/j.mcat.2023.113794

[56] Román-Leshkov, Y., Barrett, C.J., Liu, Z.Y., Dumesic, J.A. (2007). Production of dimethylfuran for liquid fuels from biomass-derived carbohydrates. *Nature*, 447(7147), 982–985. DOI: 10.1038/nature05923

[57] Hoang, A.T., Pandey, A., Huang, Z., Luque, R., Ng, K.H., Papadopoulos, A.M., Chen, W.-H., Rajamohan, S., Hadiyanto, H., Nguyen, X.P., Pham, V.V. (2022). Catalyst-Based Synthesis of 2,5-Dimethylfuran from Carbohydrates as a Sustainable Biofuel Production Route. *ACS Sustainable Chemistry & Engineering*, 10(10), 3079–3115. DOI: 10.1021/acssuschemeng.1c06363